Structural and Dynamical Properties of Ribbonlike Self-Assemblies of a Fluorinated Cationic Surfactant

E. Buhler,*,† C. Oelschlaeger,‡ G. Waton,§ M. Rawiso,§ J. Schmidt,|| Y. Talmon,|| and S. J. Candau⊥

Laboratoire de Spectrométrie Physique, UMR CNRS 5588, Université Joseph Fourier de Grenoble, B.P. 87, 38402 St. Martin d'Hères, France, Max Planck Institute for Polymer Research, Ackermannweg 10, 55021 Mainz, Germany, Institut Charles Sadron, UPR CNRS 22, 6 rue Boussingault, 67083 Strasbourg Cedex, France, Department of Chemical Engineering, Technion-Israel Institute of Technology, Haifa 32000, Israel, and I.S.I.S., Laboratoire de Chimie Supramoléculaire, 8 allée Gaspard Monge, 67083 Strasbourg Cedex, France

Received September 22, 2005. In Final Form: January 4, 2006

The structural and dynamic properties of low ionic strength micellar solutions of the cationic surfactant perfluorooctylbutane trimethylammonium bromide have been investigated by cryo-TEM, small-angle neutron scattering, small-angle X-ray scattering, T-jump and rheological experiments. The surfactant molecules self-assemble into narrow ribbons with average dimensions on the order of 4 nm × 3 nm, either under salt-free conditions or in the presence of up to 30 mM KBr or NaF. Cryo-TEM also reveals in the salt-free systems the presence of networks of multiconnected micelles. Rheological experiments showed that these surfactant systems exhibit a strong shear-thickening effect even in the presence of up to 30 mM KBr. The T-jump response of the micellar solutions was found to be multiexponential. This observation rules out the presence of only linear micelles with an exponential length distribution and suggests more complex topologies of the micellar aggregates. The relaxation time associated with the predominant process in the T-jump relaxation is strongly correlated to the critical shear rate beyond which shear thickening occurs, thus indicating that this critical shear rate is controlled by the micellar kinetics.

1. Introduction

A distinctive property of the fluorocarbon surfactants is their tendency to form structures with relatively little curvature, such as cylindrical micelles (i.e., threadlike micelles TLMs) and bilayer structures.[1,2] This is due to a higher hydrophobicity and higher stiffness of the fluorocarbon chains as compared to the same properties of hydrocarbon homologues. Furthermore, the fluorocarbon tail cross-sectional area, a_{tail}, was estimated to be 31.5 Å^2, compared to 21.4 Å^2 for the hydrocarbon, resulting in a larger packing parameter, a_{tail}/a_o, where a_o is the effective polar headgroup area.[1] This would also favor the cylindrical curvature. Therefore, one expects for such surfactants a very large end-cap energy and the formation of very long cylindrical micelles starting at very low concentrations.

In a recent study,[3] the structural and dynamic properties of low ionic strength micellar solutions of the cationic surfactant perfluorooctylbutane trimethylammonium bromide have been investigated by means of dynamic and static light scattering and rheological experiments. In the range of concentration extending from the critical micelle concentration to about the overlap concentration, C^*, the surfactant was found to self-assemble into micellar aggregates with sizes on the order of 100 nm, both under salt-free conditions and in the presence of small amounts of NaF (salt concentration $C_s < 30$ mM). At higher concentrations, the system is characterized by a single correlation length consistent with the formation of a transient network of wormlike micelles (TLMs).

The correlation length was found to drop sharply from ∼100 to ∼ 20 nm at C^*, which suggests the presence of either highly polydisperse linear or ring micellar or fractal aggregates (microgels), with an internal correlation length of ∼20 nm.

In the first part of this article, we report a study aimed at providing complementary information on the structure of the self-assemblies. The experimental techniques used were Cryo-TEM microscopy, small-angle neutron scattering (SANS), and small-angle X-ray scattering (SAXS).

The second aspect of the study concerns the dynamical properties of these systems in the vicinity of the overlap threshold, C^*, where the solutions under shear were found to exhibit complex time-dependent and history-dependent flow behaviors. In particular, the shear thickening, observed above a critical shear rate, $\dot{\gamma}_c$, for most ionic surfactants at low ionic strength[4−19] is quite

* To whom correspondence should be addressed. E-mail: eric.buhler@ujf-grenoble.fr.

† Université Joseph Fourier de Grenoble.

‡ Max Planck Institute for Polymer Research.

§ Institut Charles Sadron.

|| Technion-Israel Institute of Technology.

⊥ I.S.I.S.

(1) Wang, K.; Karlsson, G.; Almgren, M.; Asakawa, T. *J. Phys. Chem. B* **1999**, *103*, 9237.

(2) Krafft, M. F.; Giulieri, F.; Riess, J. G. *Angew. Chem., Int. Ed. Engl.* **1993**, *32*, 741.

(3) Oelschlaeger, C.; Waton, G.; Buhler, E.; Candau, S. J.; Cates, M. E. *Langmuir* **2002**, *18*, 3076.

(4) Hoffmann, H.; Platz, G.; Rehage, H.; Schorr, W.; Ulbricht, W. *Ber. Bunsen-Ges. Phys. Chem.* **1981**, *85*, 255.

(5) Rehage, H.; Hoffmann, H. *Rheol. Acta* **1982**, *21*, 561.

(6) Hoffmann, H.; Löbl, M.; Rehage, H.; Wunderlich, I. *Tenside Deterg.* **1985**, *22*, 290.

(7) Ohlendorf, D.; Interthal, W.; Hoffmann, H. *Rheol. Acta* **1986**, *25*, 468.

(8) Wunderlich, I.; Hoffmann, H.; Rehage, H. *Rheol. Acta* **1987**, *26*, 532.

(9) Hofmann, S.; Rauscher, A.; Hoffmann, H. *Ber. Bunsen-Ges. Phys. Chem.* **1991**, *95*, 2.

(10) Berwersdorff, H.-W.; Frings, B.; Lindner, P.; Oberthür, R. C. *Rheol. Acta* **1986**, *25*, 642.

(11) Lindner, P.; Bewersdorff, H.-W.; Heen, R.; Sittart, P.; Thiel, H.; Langowski, J.; Oberthür, R. C. *Prog. Colloid Polym. Sci.* **1990**, *81*, 107.

(12) Oda, R.; Panizza, P.; Schmutz, M.; Lequeux, F. *Langmuir* **1997**, *13*, 6407.

(13) Liu, C. H.; Pine, D. J. *Phys. Rev. Lett.* **1996**, *77*, 2121.

(14) Boltenhagen, P.; Hu, Y.; Matthys, E. F.; Pine, D. J. *Phys. Rev. Lett.* **1997**, *79*, 2359.

(15) Berret, J. F.; Gamez-Corrales, R.; Oberdisse, J.; Walker, L. M.; Lindner, P. *Europhys. Lett.* **1998**, *41*, 677.

10.1021/la0525832 CCC: $33.50
Published on Web 02/07/2006

large for the fluorocarbon surfactant solutions, even at concentrations close to the cmc, as compared to that for hydrocarbon analogues.[3,6,20] The major difficulty encountered in the attempts to explaining the above effect concerns the values of the critical shear rate, $\dot{\gamma}_c$. In the models initially proposed, shear thickening was attributed to shear-induced alignment, causing the end-to-end fusion of small rodlike micelles (TLMs), leading to the formation of a network of long micelles.[9,21,22]

The presence of monodisperse particles small enough not to overlap at $C < C^*$ was commonly accepted on the basis of theoretical predictions[23] and small-angle neutron scattering (SANS) results, compatible with rod lengths of several tens of nanometers.[12,14,22] In the above model, shear-induced gelation occurs when the shear rate becomes comparable to the rotational diffusion constant of the micellar rods in the quiescent system. In fact, as pointed out by several authors, the measured critical shear rates, $\dot{\gamma}_c$, are several orders of magnitude lower than the rotational diffusion rates calculated for rods with sizes of several tens of nanometers.[9,12,15]

Recently, two new mechanisms for the formation of shear-induced structures were proposed. The first one assumes that electrostatic correlation−attractions lead to the formation of metastable bundles.[24] Under shear flow at shear rates, $\dot{\gamma}$, larger than the unbinding time of the micelles, the bundles form and grow in thickness. For solutions of sufficiently high concentration that are still unentangled, the micelles should aggregate into a network of bundles.

The second mechanism proposed is a ring-driven scenario.[25] The presence of micellar rings at $C < C^*$ is expected theoretically in the limit of high end-cap energy for the micelles. According to the model, the linking and delinking kinetics of large rings controls the shear-thickening process. Equilibrium between rings and open chains in turn controls the slow relaxations.

Both of these mechanisms require the presence of large particles (bundles or large rings) in the quiescent solutions at $C < C^*$. Such large entities were detected in recent studies.[3,26−28] It was also shown that $\dot{\gamma}_c$ does not depend on the cell geometry and is therefore a micellar characteristic.[3]

Another challenging observation is the structural memory that persists for a very long time after a mechanical or thermal perturbation.[3,18] This was explained by assuming that the perturbation induces a change in the number of chains present in the solution and that the slow relaxation toward equilibrium is controlled by reversible scission kinetics.[25] Reversible scission is the only micellar reaction that can alter the total number of chains present in the system. If it is much slower than stress relaxation, then this will give structural memory that extends far beyond the time scales of flow response.

The fact that the structural relaxation is faster in the presence of salt can be explained by faster reversible scission kinetics, as shown by T-jump experiments.[29]

The second part of this article describes rheological and T-jump experiments performed on perfluorooctylbutane trimethylammonium bromide solutions in the presence of KBr. We found that the addition of moderate amounts of this salt does not reduce shear-thickening, contrary to the effects of other salts that exhibit a weaker binding to the surfactant. This allowed us to obtain for the first time both T-jump and shear-thickening results under the same conditions. These results show a net correlation between $\dot{\gamma}_c$ and a characteristic T-jump relaxation time.

2. Materials and Methods

2.1. Sample Characteristics. The perfluorooctylbutane trimethylammonium bromide [$C_8F_{17}(CH_2)_4N^+(CH_3)_3Br^-$ ($M = 614$ g/mol)] surfactant (C_8F_{17}) has been synthesized using a method involving four steps, as described in ref 3. The sample solutions were prepared by gently stirring the surfactant in deionized water for 3 days. For equilibrium measurements, they were stored for at least 2 days at the desired temperature prior to measurements. Throughout the article, the concentrations are expressed in g·cm^{-3}.

2.2. Cryo-TEM. Vitrified specimens for cryogenic-temperature transmission electron microscopy (cryo-TEM) were prepared in a controlled environment vitrification system (CEVS) at 25 °C and 100% relative humidity, as previously described.[30,31] In brief, a drop of the solution to be imaged was applied to a perforated carbon film, supported on an electron microscopy copper grid, held by CEVS tweezers. The sample was blotted with filter paper and immediately plunged into liquid ethane at its freezing point (−183 °C). The vitrified samples were then stored under liquid nitrogen (−196 °C), transferred to an Oxford CT3500 cooling holder via its "work station", and kept in a Philips CM120 microscope at about −180 °C. Images were recorded at a 120 kV acceleration voltage, in low-dose mode, to minimize electron-beam radiation damage. We used a Gatan MultiScan 791 cooled CCD camera, with the Digital Micrograph 3.1 software package, to acquire the images. Images were recorded at a nominal underfocus of about 2 μm to enhance phase contrast.

2.3. Small-Angle X-ray Scattering. All experiments were carried out at $T = 30$ °C with a Nanostar small-angle X-ray scattering spectrometer (Bruker-Anton Paar). The samples were held in calibrated mica cells of 1 mm thickness to avoid multiple scattering and were maintained in an oven with temperature regulation better than 0.01 °C.

The Nanostar spectrometer operates with a pinhole collimator and a wire proportional gas detector. A monochromatic ($\lambda = 1.54$ Å, Cu Kα_1) and almost parallel beam (divergence = 0.03°) is obtained through two Gobel crossed mirrors. The size of the incident beam on the sample is close to 300 μm. The sample-to-detector distance was set at 0.2 m (0.06 Å^{-1} < q < 0.9 Å^{-1}), and the q resolution was 0.005 Å^{-1}. The scattering wave vector, q, is defined by eq 1, where θ is the scattering angle.

$$q = \frac{4\pi}{\lambda} \sin \frac{\theta}{2} \tag{1}$$

2.4. Small-Angle Neutron Scattering. SANS experiments were carried out on the D11 spectrometer at the Laue Langevin Institut at Grenoble (ILL, France). The chosen incident wavelength, λ, depends on the set of experiments as follows. For a given wavelength, the range of the amplitude of the transfer wave vector, q, was selected by changing the sample-to-detector distance, D. Three sets of sample-to-detector distances and wavelengths were chosen ($D = 2$ m, $\lambda = 6 \pm 0.5$ Å; $D = 8$ m, $\lambda = 6 \pm 0.5$ Å; and $D = 28$ m, $\lambda = 6 \pm 0.5$ Å) so that the following q ranges were available, respectively: 3.66

(16) Keller, S. L.; Boltenhagen, P.; Pine, D. J.; Zasadzinski, J. A. *Phys. Rev. Lett.* **1998**, *80*, 2725.
(17) Gamez-Corrales, R.; Berret, J.-F.; Walker, L. M.; Oberdisse, J. *Langmuir* **1999**, *15*, 6755.
(18) Berret, J.-F.; Gamez-Corrales, R.; Lerouge, S.; Decruppe, J.-P. *Eur. Phys. J. E* **2000**, *2*, 343.
(19) Hu, Y. T.; Matthys, E. F. *J. Rheol.* **1997**, *41*, 151.
(20) Stähler, K.; Selb, J.; Candau, F. *Colloid Polym. Sci.* **1998**, *276*, 860.
(21) Cates, M. E.; Turner, M. S. *Europhys. Lett.* **1990**, *7*, 681.
(22) Wang, S. Q.; Gelbart, W.; Ben-Shaul, A. *J. Phys. Chem.* **1990**, *94*, 2219.
(23) Mackintosh, F.; Safran, S.; Pincus, P. *Europhys. Lett.* **1990**, *12*, 697.
(24) Barentin, C.; Liu, A. J. *Europhys. Lett.* **2001**, *55*, 432.
(25) Cates, M. E.; Candau, S. J. *Europhys. Lett.* **2001**, *55*, 887.
(26) Weber, V.; Schosseler, F. *Langmuir* **2002**, *18*, 9705.
(27) Weber, V.; Narayanan, T.; Mendes, E.; Schosseler, F. *Langmuir* **2003**, *19*, 992.
(28) Bernheim-Groswasser, A.; Zana, R.; Talmon, Y. *J. Phys. Chem. B* **2000**, *104*, 405.
(29) Oelschlaeger, C.; Waton, G.; Candau, S. J.; Cates, M. E. *Langmuir* **2002**, *18*, 7265.
(30) Bellare, J. R.; Davis, H. T.; Scriven, L. E.; Talmon, Y. *J. Electron. Microsc. Technol.* **1988**, *10*, 87.
(31) Talmon, Y. Cryogenic Temperature Transmission Electron Microscopy in the Study of Surfactant Systems. In *Modern Characterization Methods of Surfactant Systems*; Binks, B. P., Ed.; Marcel Dekker: New York, 1999; Chapter 5, pp 147−178.

$\times 10^{-2} \leq q$ (Å^{-1}) $\leq 1.86 \times 10^{-1}$, $9.16 \times 10^{-3} \leq q$ (Å^{-1}) $\leq 4.71 \times 10^{-2}$, and $1.62 \times 10^{-3} \leq q$ (Å^{-1}) $\leq 1.35 \times 10^{-2}$. Measured intensities were calibrated to absolute values (cm^{-1}) using the normalization by the attenuated direct beam classical method. Standard procedures to correct the data for the transmission, detector efficiency, and backgrounds (solvent, empty cell, electronic, and neutron background) were carried out.

2.5. Viscosimetry. The rheological measurements were performed with two different devices:

1. A Rheometrics RFS II fluid spectrometer, using cone-plate geometry. The cell has a gap of 0.045 mm, an angle of 0.035 rad, and a diameter of 50 mm.

2. A Low Shear 30 viscometer using Couette geometry. The Couette cell has a gap of 0.5 mm and a height of 20 mm.

Both experiments were carried out with imposed strain equipment; special care was taken to avoid water evaporation.

Viscosimetry measurements allowed us to determine the overlap concentration, C^*, separating the dilute from the semidilute regime and corresponding to the concentration at which we observe a strong increase in the viscosity with the C_8F_{17} concentration. $C^* = 0.5 \times 10^{-2}$ g/cm^3 for [KBr] = 30 mM and $T = 30$ °C, whereas $C^* = 1.5 \times 10^{-2}$ g/cm^3 for [NaF] = 20 mM and for salt-free solutions.

2.6. T-Jump Device. The T-jump device has been described elsewhere.[29,32] For T-jump measurements, the surfactant solutions were filtered through a 0.22 μm Millipore filter. The temperature jump is produced by means of the discharge of a capacitor through the sample. The rise time of the T-jump is 1 μs; its amplitude is calculated from the values of the stored electrical energy and the heat capacity of the sample; and it can be varied between 0.1 and 2 °C. The scattering cell is illuminated by an intense light beam obtained from a powerful (150 W) mercury−xenon lamp in conjunction with a large-aperture condenser (Oriel Aspherab). Several interference filters allow for the selection of the following wavelengths: 313, 365, 405, 436, 546, and 577 nm. A fraction of the incident light beam is sent to the photodiode, which then delivers a reference signal. An electronic device uses this signal to compensate for lamp power or arc position instabilities.

Two photomultipliers (PM) are used for the detection of the light scattered at 90 and 20°. A photodiode placed on the optical axis measures the transmitted light.

The PM signal is digitalized and acquired using a pseudo-logarithmic time base in which the sampling time is periodically increased. For each measurement, several relaxation functions are summed to obtain an averaged curve. This results in further improvement to the signal/noise ratio. After the T-jump, the temperature in the cell decreases slowly and may be considered to be constant after 5 s. The temperature in the cell is controlled to ±0.1 °C.

3. Results and Discussion

3.1. Structural Properties. Cryo-TEM experiments were performed on C_8F_{17} solutions at a concentration of $C = 1.5 \times 10^{-2}$ g/cm^3 both under the salt-free condition and in the presence of 20 mM NaF. This surfactant concentration corresponds approximately to the crossover concentration between dilute and semidilute regimes.[3] Figure 1 show micrographs of vitrified solutions containing 20 mM NaF. Figure 1a shows ribbons with some sections (black arrow) seen from the side, giving a higher optical density. White arrow points to twists that are seen as black dots. Similar structures are observed in Figure 1b. Note how a ribbon twists in Figure 1b. The white arrowheads indicate the section that is seen face-on, whereas the black arrowheads indicate the sections seen from the side. The behavior without salt is more complicated, as shown in the micrographs of Figure 2. Here we see a dense network of interconnected micelles (white arrowheads) in addition to twisted ribbonlike micelles (Figure 2a). The white arrows indicate patches of those networks seen from the side. Figure 2b shows well-aligned ribbons that are probably due to the thinning of the liquid specimen during preparation; note the changes in optical density along the ribbons as they twist. Figure 2c shows clearly how the above-shown networks form on the ribbons (white arrows). The black arrow is used to emphasize that the size of the "loops" in the network is not constant but is always rather small. A single free loop or ring is also seen in the upper left corner of the micrograph.

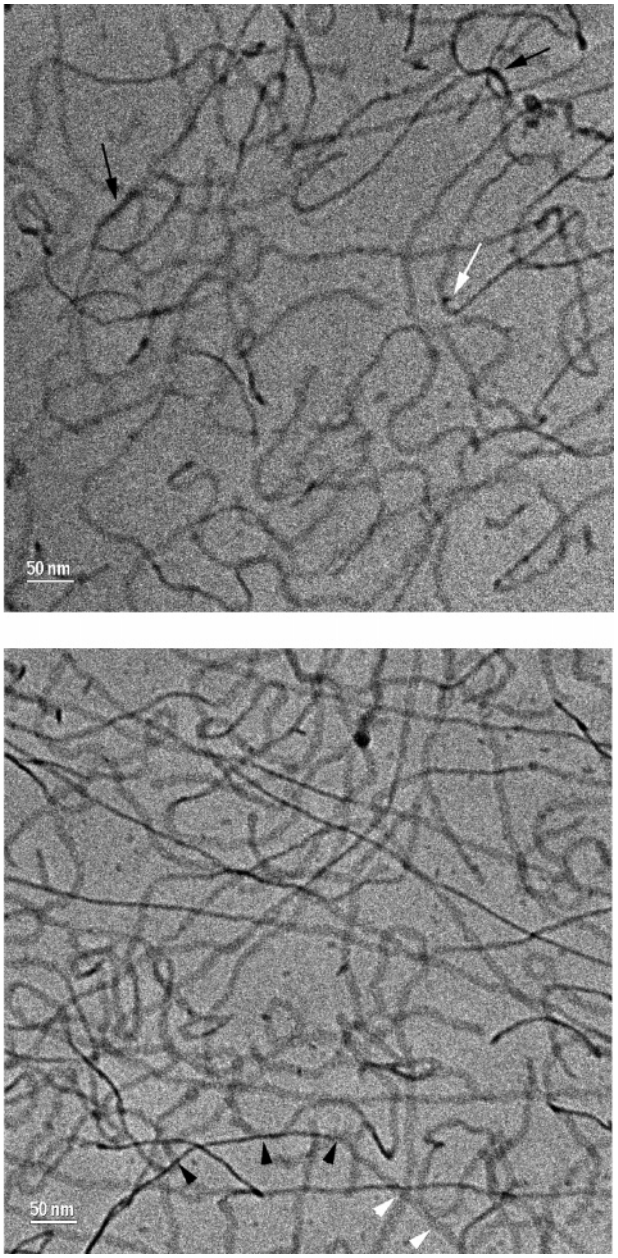

Figure 1. Cryo-TEM images of $C = 1.5 \times 10^{-2}$ g/cm^3 C_8F_{17} solutions in the presence of 20 mM NaF. (a) Black arrow indicates ribbons with some sections seen from the side; white arrow shows twists or sharp bends. (b) Twist of a ribbon: white arrowheads indicate a section that is seen face-on, whereas black arrowheads indicate the sections seen from the side.

A common observation in all these micrographs is that the fluorocarbon surfactant does not form cylindrical micelles as we expected but instead forms thin ribbons with a relatively well-defined width on the order of 15 nm. This surprising result may come from a compromise between the preference of the rigid fluorinated tails to form bilayers and the effect of the polar heads and the four CH_2 spacers that favor cylindrical curvature.

(32) Faetibold, E.; Waton, G. *Langmuir* **1995**, *11*, 1972.

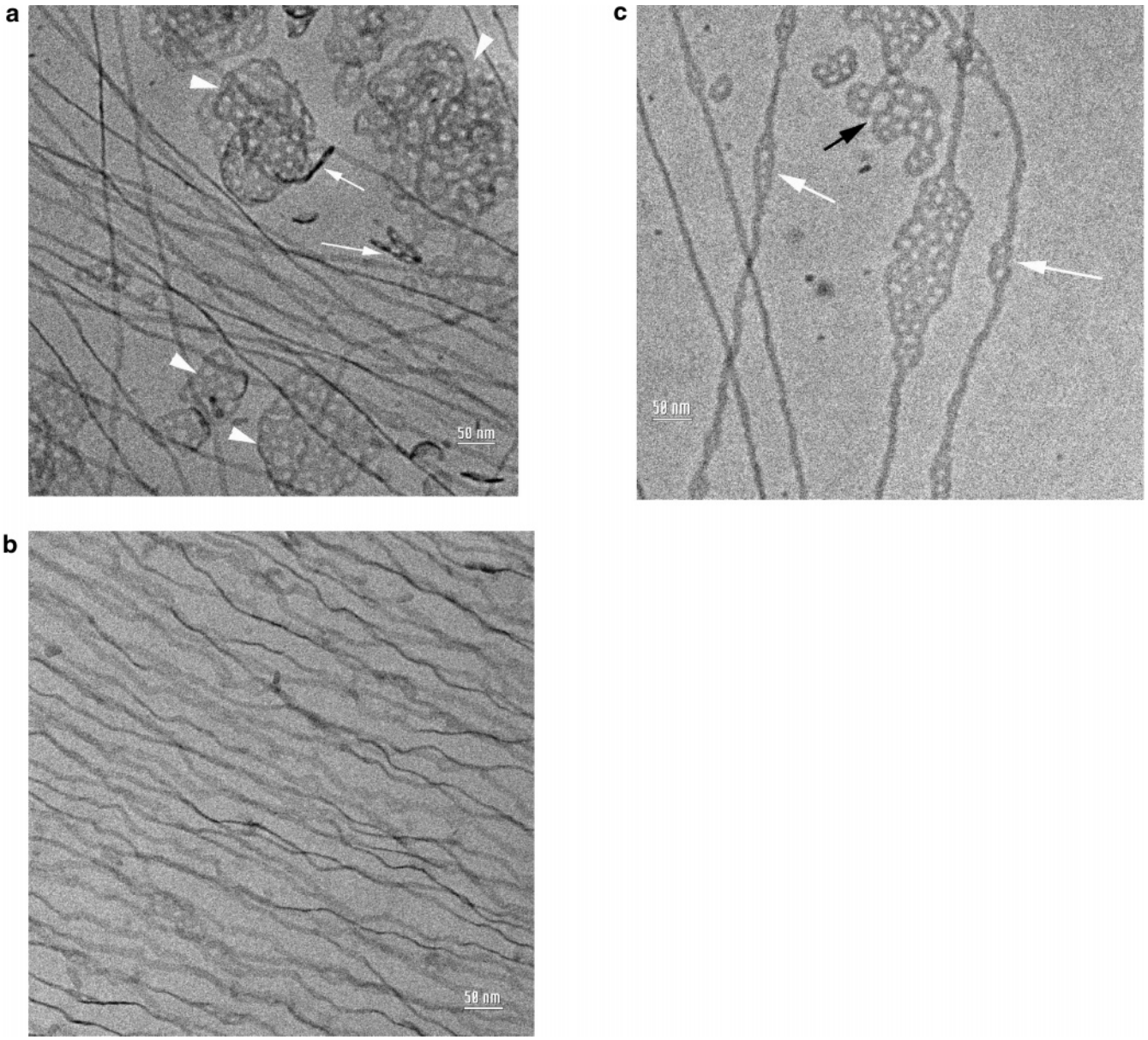

Figure 2. Cryo-TEM images of the structure of C_8F_{17} salt-free solutions with $C = 1.5 \times 10^{-2}$ g/cm^3. (a) White arrowheads show dense networks of interconnected micelles in addition to twisted ribbonlike micelles. The white arrows indicate patches of those networks seen from the side. (b) Well-aligned ribbons. (c) White arrows indicate loops of micelles formed on the ribbons; the black arrow indicates small network segments.

The second interesting piece of information concerns the existence of networks of multiconnected micelles in the salt-free systems. This observation must be connected to the results of the light scattering study that suggested the presence in the same systems of aggregates of size ~100 nm and an internal correlation length of 20 nm.[3] The contour length of the loops observed in the micrographs is in the range of 100 nm, that is, about twice the persistence length determined in the light-scattering experiments. The aggregates shown in the micrographs reveal a bidimensional aspect underlined by the fact that the network cells appear as holes. It must be noted that it is very difficult to obtain images of large structures in cryo-TEM because the vitrified film is very thin (10−300 nm) and large particles are flattened. Nevertheless, the micrographs of Figure 2a and c seem to indicate the presence of patches of perforated lamellae. In the quiescent state, these lamellae would be crumpled and would form isotropic tridimensional objects. In addition to the deformation due to the film thickness, one should keep in mind effects of the flow due to the blotting when preparing the films.[30,31] Thus, the micrographs may give instantaneous pictures of the system at different stages of the flow-induced deformation. That is what we observe in the micrograph in Figure 2c: a very stretched aggregate transforming into a ribbon still containing segments of network. The micrograph in Figure 2b shows a deformation state where all of the material has been transformed into shear-aligned ribbons.

In the presence of salt, the system behaves as an entangled micellar solution, which suggests that the concentration is slightly above C^*. One must also note the enhanced flexibility of the ribbons.

Because cryo-TEM does not allow us to determine the width and the thickness of the ribbon accurately, we have attempted to measure these parameters by SANS and SAXS.

Figure 3 shows scattering curves $I(q)$ for three C_8F_{17} solutions in deuterated water at a concentration of $C = 1.5 \times 10^{-2}$ g/cm^3, without salt, and in the presence of 20 mM NaF and 30 mM KBr. The scattering curve of the salt-free system exhibits the typical interaction peak of polyelectrolyte solutions. The peak occurs at a q value inversely proportional to the average distance between

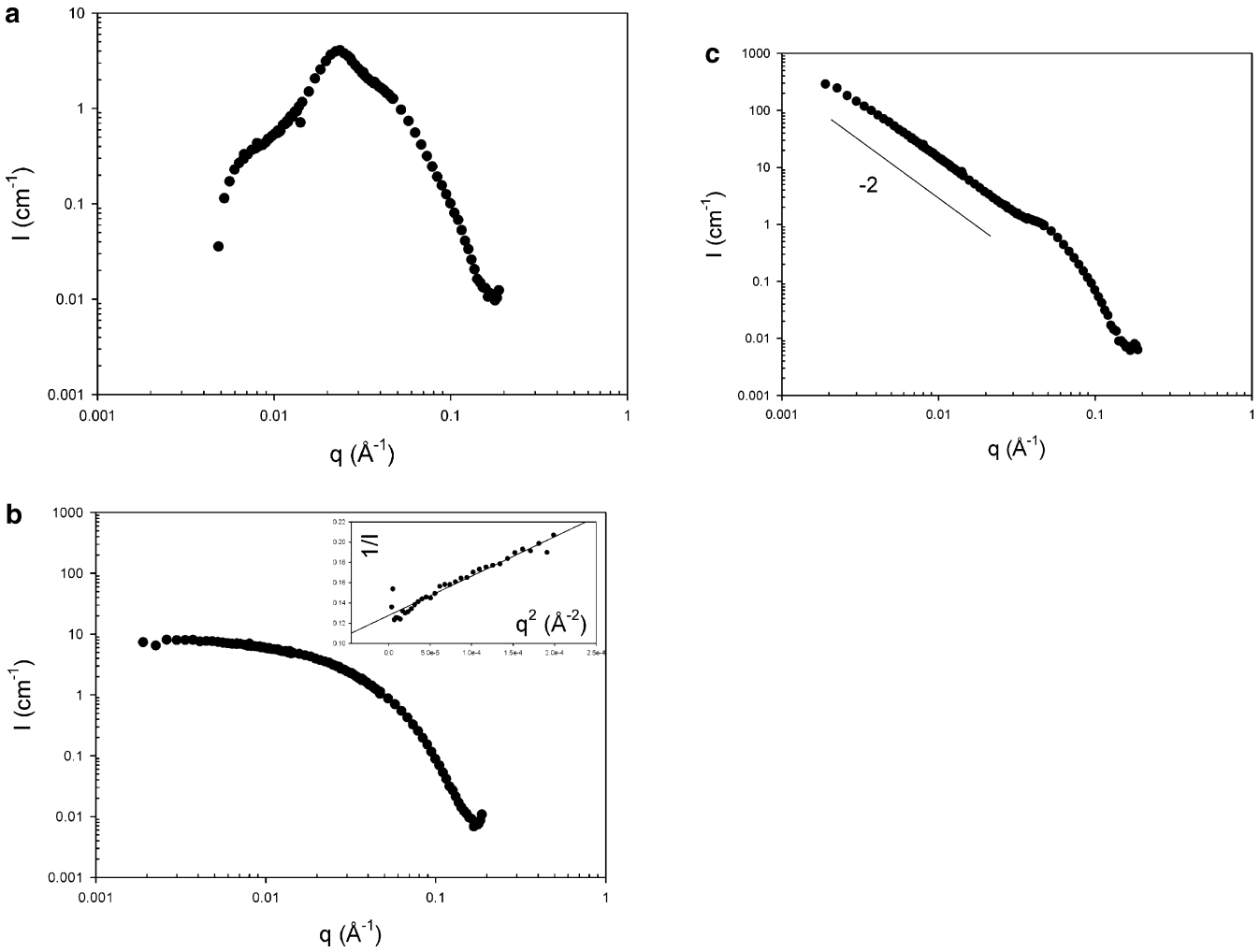

Figure 3. Variation of the scattering intensity, I, with q obtained by SANS in $C = 1.5 \times 10^{-2}$ g/cm^3 C_8F_{17} solutions: (a) without salt ($T = 20$ °C); (b) in the presence of 20 mM NaF ($T = 20$ °C); and (c) in the presence of 30 mM KBr ($T = 30$ °C).

the overlapping linear aggregates. In the high-q regime, one can distinguish another weak oscillation that is likely associated with the sharp interface between micellar aggregates and the solvent. The interaction peak has disappeared in the scattering curve of the sample containing 20 mM NaF (cf. Figure 3b) because of the electrostatic screening produced by the presence of the salt (cf. Figure 3a). The low-q part of $I(q)$ can be fitted by the Ornstein−Zernicke law

$$\frac{1}{I(q)} = \frac{1}{I(0)}(1 + q^2\xi^2) \qquad (2)$$

where ξ is the correlation length. From the plot of I^{-1} versus q^2 (cf. inset), one obtains $\xi = 5.5$ nm, in agreement with previous findings from dynamic light scattering experiments.[3] In the high-q range, one still observes an oscillation of the scattered intensity. The scattering curve of the sample containing 30 mM KBr does not exhibit a Guinier regime with a plateau of the scattered intensity at low q but instead a q^{-2} behavior in a rather extended q range, followed by a narrow q^{-1} regime and by the high-q oscillation (cf. Figure 3c). The absence of a Guinier regime indicates that, in this system, the correlation length is larger than in the sample with 20 mM NaF. This may be due to the enhanced flexibility of the linear micellar aggregates, resulting from both a larger salt concentration and a stronger binding of the Br^- ions as compared with that of the F^- ions.

Figure 4 shows the Porod representation of $q^4I(q)$ versus q for the three systems. This representation was used because it allows us to emphasize the q^{-4} decrease that is characteristic of particles with sharp interfaces and the oscillating terms, related to the shape of the particle cross section, of the feature in which we are interested. The curves of Figure 4 exhibit a single oscillation with a maximum and a minimum occurring at the same values of q for the three systems investigated. This observation clearly indicates that the local structure is the same for the three systems.

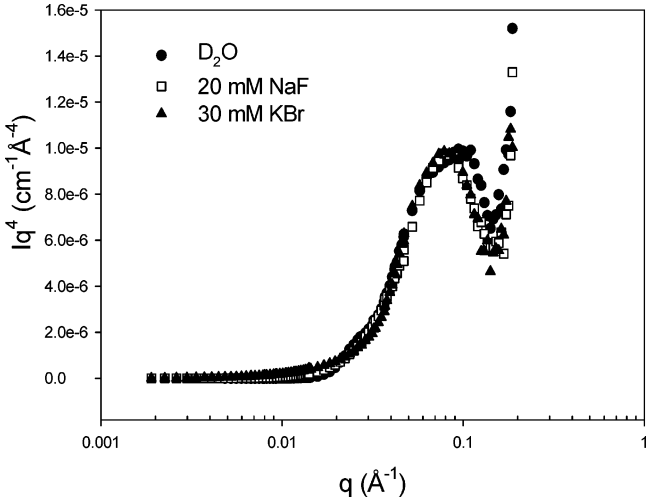

Figure 4. Porod representation of the form factors of $C = 1.5 \times 10^{-2}$ g/cm^3 C_8F_{17} self-assemblies without salt (●), in the presence of 20 mM NaF (□), and in the presence of 30 mM KBr (▲).

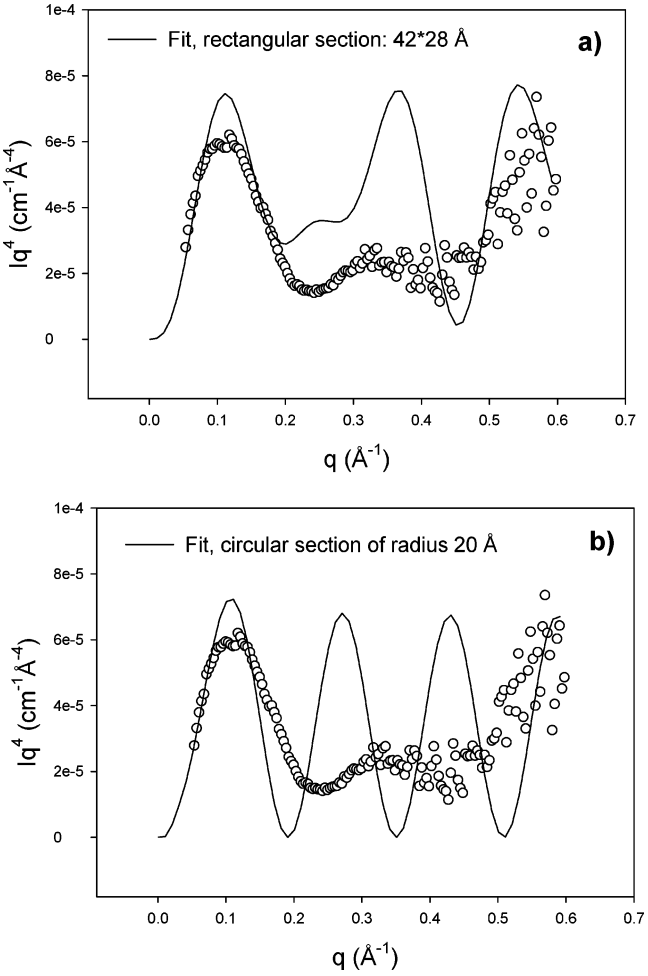

Figure 5. Porod representation of the form factor of $C = 5 \times 10^{-2}$ g/cm^3 C_8F_{17} self-assemblies in the presence of 30 mM KBr at $T = 30$ °C. The black line represents the calculated curve (a) for a ribbon with a rectangular section of 42 Å × 28 Å and (b) for a circular section of radius $R = 20$ Å.

However, the absence of a second oscillation at higher q prevented us from determining the cross-sectional dimensions of the micellar aggregates. Therefore, we turned to SAXS experiments. To increase the scattering intensity, we investigated a more concentrated H_2O solution ($C = 5 \times 10^{-2}$ g/cm^3) in the presence of 30 mM KBr at $T = 30$ °C. The scattering curves obtained for this sample are plotted in the Porod representation in Figure 5. The maximum of the first oscillation is found for a q value slightly larger than in the SANS curves of Figure 4 ($q_{max} = 0.08-0.09$ Å^{-1} for SANS and $q_{max} = 0.1$ Å^{-1} for SAXS). This might be either a concentration effect or an isotopic effect. We have also plotted in Figure 5 the best fits to the data of the theoretical form factors for a rigid rod with a rectangular section (Figure 5a) and with a circular section (Figure 5b).[33] If the section is circular, with a radius R, then the form factor $P(q)$ can be written as in eq 3. J_1 is the first-order Bessel function, and L is the length of the rod. For a rectangular section,[33] it is given by eq 4 where a and b are the half side lengths of the rectangle.

$$P(q) = \frac{\pi}{qL}\left(\frac{2J_1(qR)}{qR}\right)^2 \quad (3)$$

$$P(q) = \frac{\pi}{qL}\frac{2}{\pi}\int_0^{\pi/2}\left(\frac{\sin(qa\cos\beta)}{qa\cos\beta}\frac{\sin(qb\sin\beta)}{qb\sin\beta}\right)^2 d\beta \quad (4)$$

Despite the large scattering of the data, a better fit is definitively obtained for a rectangular section with a width of 42 Å and a thickness of 28 Å. These values are in reasonable agreement with the estimates determined from the micrographs. The damping of the second oscillation might result from the width polydispersity.

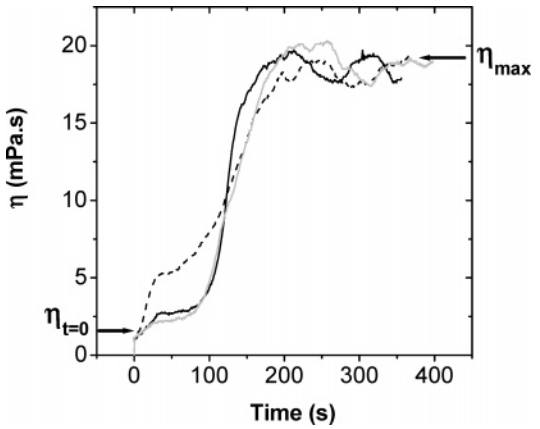

Figure 6. Time dependence of the solution viscosity with $C = 0.25 \times 10^{-2}$ g/cm^3, [KBr] = 15 mM, and $T = 30$ °C. The dark line is obtained for an equilibrium solution and for a shear rate of 20 s^{-1}, whereas the dashed line and the lighter line were obtained after resting times of 120 and 300 s, respectively.

3.2. Dynamic Properties. *Rheological Experiments.* It has been shown in a previous study[3] that salt-free aqueous solutions of C_8F_{17} exhibit strong shear thickening (up to 50 times) above a critical threshold of shear rate, $\dot{\gamma}_c$, in the concentration range cmc $\leq C \leq C^*$. The stress increase occurs after a latency time following the onset of steady shear. Then, the stress evolves slowly over very long periods of times (up to hours) before achieving steady state. A similarly slow time scale controls the disappearance of structural memory. Furthermore, the transient mechanical response depends drastically on the thermal history of the sample.[3]

The addition of a screening salt such as NaF to the C_8F_{17} solution produces a decrease in the amplitude of shear thickening, whereas the critical shear rate increases with salt concentration.

The same effects are produced by an increase in temperature. The above features were also observed for other surfactant systems.[15,17]

In the present study, we have investigated C_8F_{17} solutions in the presence of KBr. The Br^- ions are known to bind strongly to the surfactant, thus modifying the topology of the micellar aggregates, as clearly indicated by a lower overlap concentration C^*, as compared to that of systems containing no salt or NaF.

An illustration of the shear-thickening effect occurring in these systems is given in Figure 6, which shows responses to steady flow with $\dot{\gamma} = 20$ s^{-1} for solutions at $C = 0.25 \times 10^{-2}$ g/cm^3 ($C/C^* \approx 0.5$) in the presence of 15 mM KBr and $T = 30$ °C. The measurements were performed first on a sample left to stand in the cell for a long time after it had been delicately poured into the cell in order to reach equilibrium conditions (dark curve in Figure 6). The typical response described above is observed with a latency time of 80 s and a ratio of the maximum viscosity, η_{max}, over the viscosity at zero time, $\eta_{t=0}$, on the order of 20. This value of $\eta_{max}/\eta_{t=0}$ is quite large and comparable to that obtained for a salt-free system at the same C/C^* ratio, temperature, and $\dot{\gamma}$.[3] Under the same conditions, systems with 15 mM NaF do not exhibit any shear thickening.

Another feature common in systems either with or without KBr concerns the memory effects following a mechanical perturbation. Figure 6 also shows the responses to steady flow

(33) Mittelbach, P.; Porod, G. *Acta Phys. Aust.* **1961**, *14*, 185.

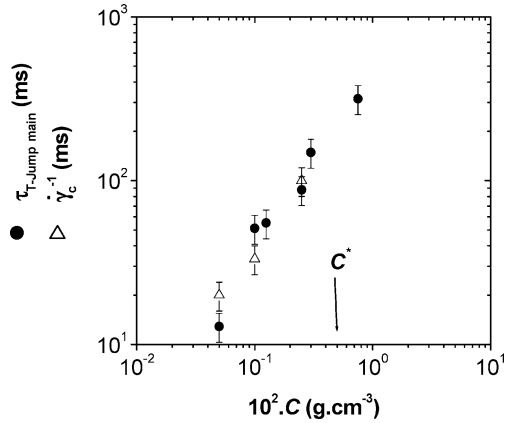

Figure 7. Variation of the main T-Jump characteristic time, τ_{TJmain}, (●) and of the inverse of the critical shear rate (△) as a function of the C_8F_{17} concentration in the presence of 30 mM KBr at $T = 30$ °C.

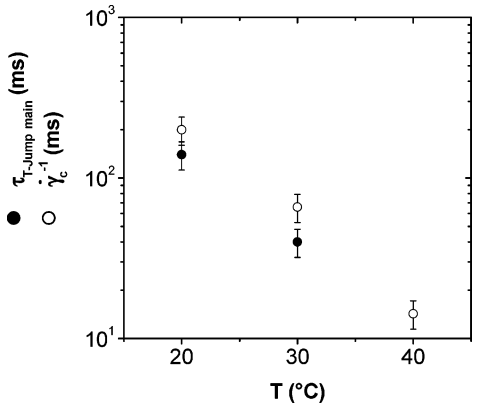

Figure 8. Variation of the main T-jump characteristic time, τ_{TJmain}, (●) and of the inverse of the critical shear rate (○) as a function of the temperature for $C = 0.25 \times 10^{-2}$ g/cm^3 solutions in the presence of 15 mM KBr.

obtained by the following procedure: the sample is presheared at $\dot{\gamma} = 20$ s^{-1} until the viscosity plateau, η_{max}, is reached, and then the shearing is stopped and resumed at the same shear rate after a resting time. If the latter is 120 s, then the shape of the shear-increased variation (dashed curve) is different from that obtained for the sample at equilibrium (dark curve), in particular, half the latency time. If the resting time is 300 s, then the shear viscosity variation corresponding to a sample initially at equilibrium is recovered. Experiments of shear cycling with variable periods led to a value of the memory time of ∼200−300 s. Also, the analysis of the stress relaxation following the suppression of the shear, once the plateau η_{max} is established, provided a measure of the stress relaxation time of ∼20 s for this sample.

We have also investigated the effects of surfactant concentration, C, temperature, T, and KBr content on the critical shear rate, $\dot{\gamma}_c$, of the C_8F_{17} solutions. The results are given in Figures 7−9, giving the variations of $\dot{\gamma}_c^{-1}$ versus C, T, and [KBr], respectively. The critical shear rate is found to vary significantly with surfactant concentration (Figure 7) and temperature (Figure 8) for systems with a given KBr content. These observations are in agreement with previously reported results on other systems.[3,26,29,34] In contrast, the effect of KBr on $\dot{\gamma}_c$ is quite different from that obtained with weaker binding salts such as NaF.

(34) Candau, S. J., Merikhi, F.; Waton, G.; Lemaréchal, P. *J. Phys. (Orsay, Fr.)* **1990**, *51*, 977.

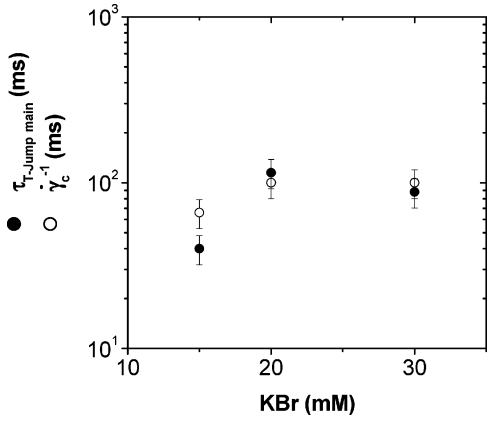

Figure 9. Variation of the main T-jump characteristic time, $\tau_{TJ\ main}$, (●) and of the inverse of the critical shear rate (○) as a function of the KBr content at $C = 0.25 \times 10^{-2}$ g/cm^3 and $T = 30$ °C.

In the latter case, $\dot{\gamma}_c$ was found to increase drastically with salt content, and it was believed that this large increase, up to the experimental limit, was at the origin of the disappearance of shear thickening at high salt content.[25] For the C_8F_{17} solutions in the presence of KBr, Figure 9 shows that the variation of $\dot{\gamma}_c$ with [KBr] is limited and complex.

Kinetic Properties. The kinetic properties were investigated through the response of the scattered intensity to a T-jump. Joule heating by means of a capacitor discharge produces the T-jump; therefore, it requires the presence of salt in the solution. In solutions containing NaF, no detectable signal could be obtained. In contrast, the KBr aqueous solutions of C_8F_{17} provide a rather large T-jump response, as shown in Figure 10, that has been obtained for a sample with $C = 0.25 \times 10^{-2}$ g/cm^3, [KBr] = 30 mM, and $T = 30$ °C. The curve representing the decay of the scattering intensity after the T-jump is clearly multiexponential. In the short time range ($t < 5$ ms), a first decay of small amplitude is observed. This mode occurs generally in systems with $C \geq C^*$ and corresponds to a cooperative diffusion mode with a characteristic time varying as q^{-2}.[29] In the present case, this short time decay could be associated with internal modes of aggregates of multiconnected ribbons. At longer times, the decay of scattering intensity cannot be fitted by a single exponential, as shown in Figure 10, but by an exponential with a well-defined characteristic time ($\tau_{TJ,main} \approx 90$ ms in the example of Figure 10) and a tail, with an amplitude of ∼25% of the total amplitude, that extends far beyond the time scales available with a conventional T-jump setup. To study this slow process, we have set up a slow T-jump device allowing the investigation of longer time scales. A temperature increase of 3.5 °C is obtained by Joule heating, using alternating current with frequency of ∼10 kHz. The rise time of the T-jump is ∼20 s as shown in Figure 11. In the same Figure, we report the T-jump response for an aqueous solution of C_8F_{17} at $C = 0.25 \times 10^{-2}$ g/cm^3, with 20 mM KBr and $T = 30$ °C. A single-exponential fit, obtained after discarding the first 20 seconds, provides a relaxation time of $\tau_{TJ\ slow} = 235$ s that is on the order of magnitude of the memory time of the system.

The above behavior differs from that reported in previous T-jump studies in which a single-exponential decay was observed.

A theoretical model was derived to describe the T-jump relaxation of a system of linear equilibrium polymers undergoing a scission-recombination process.[21] The model predicts that after a T-jump the average micellar length decreases exponentially toward its new equilibrium value, with a characteristic time equal to half the breaking time. As a matter of fact, the observation of a single-exponential T-jump signal, combined with a theoreti-

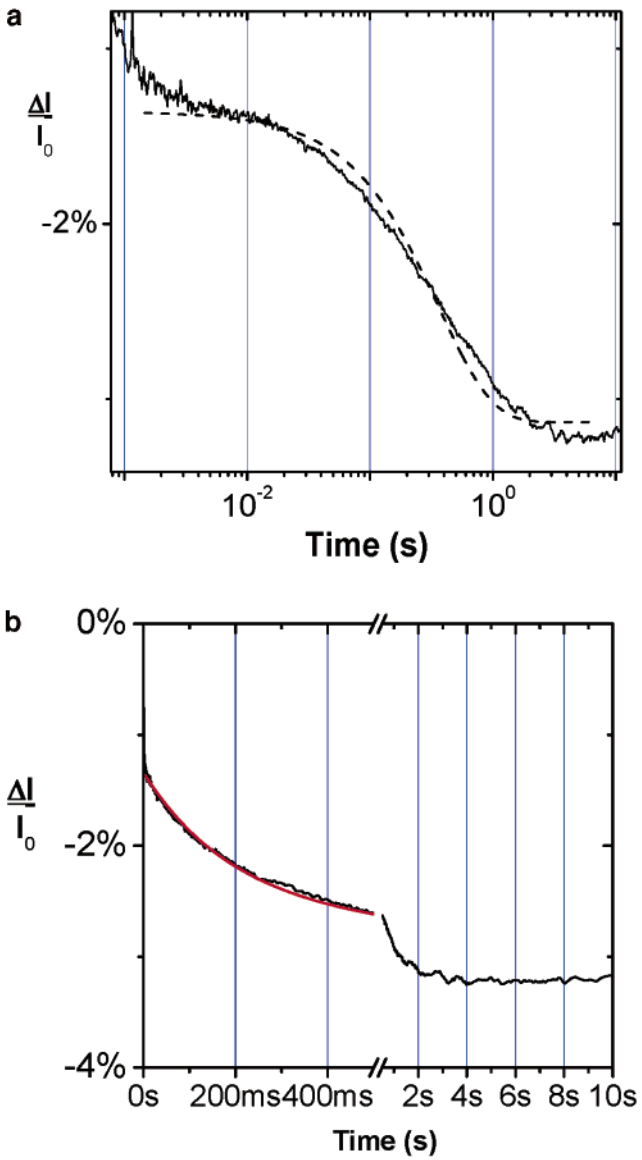

Figure 10. T-jump responses for solutions with $C = 0.25 \times 10^{-2}$ g/cm^3, $T = 30$ °C, and [KBr] = 30 mM. (a) The dashed line represents a single-exponential function. (b) Linear representation of the T-jump response; the continuous line represents the fit of the response curve.

cally predicted variation of τ_{TJ} like $\tau_{TJ} \approx C^{-1/2}$, is generally considered to be the unambiguous signature of a population of linear chains undergoing reversible scission.

On the contrary, the observation of nonexponential behavior suggests a more complex topology of the micellar aggregates. Indeed, if either micellar rings or microgels are present in solution in addition to linear chains, as suggested by light-scattering experiments performed in solutions containing no salt or NaF,[3] other micellar reactions could contribute in T-jump experiments. For instance, bond interchange can create one ring and one chain out of one chain only or create two rings out of one (or vice versa). One can also envision the fusion and breakdown of the gel fragment, which would be a mechanism quite similar to that of a gel formed by the topological interlinking of rings. In any case, the reversible scission is the only mechanism that can alter the total number of chains present in the system. It was suggested previously that the time, τ_{break}, associated with this process could become very long at low salt content and be responsible for the memory effect. To explain the behavior illustrated by Figure 10, it could be speculated that the main relaxation process is the

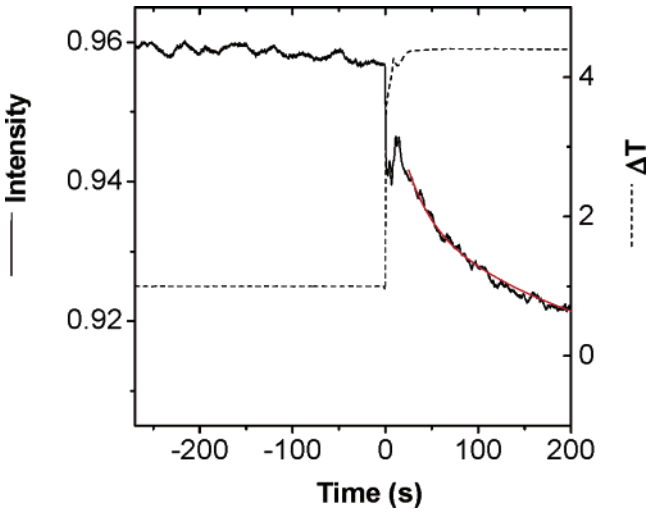

Figure 11. T-jump response for solutions with $C = 0.25 \times 10^{-2}$ g/cm^3 and [KBr] = 20 mM at $T = 30$ °C. The continuous line represents the fit of the data, whereas the dashed line represents the T-jump.

fusion-recombination of micellar aggregates with different topologies, whereas the slowest relaxation process is the reversible scission of linear chains.

Figures 7−9 show the variations of τ_{TJmain} as a function of C, T, and [KBr]. A striking feature is the correlation between τ_{TJmain} and the inverse of the critical shear rate, $\dot{\gamma}_c$. These results show unambiguously that $\dot{\gamma}_c$ is associated with a micellar kinetics process. It must also be noted that it is the first time that a T-jump relaxation time is found to increase with surfactant concentration (cf. Figure 7), thus confirming that the corresponding relaxation process cannot be ascribed to the reversible scission of linear chains.

4. Conclusions

This article outlines novel experimental observations on both the structure and the dynamics of micellar solutions of the fluorinated cationic surfactant C_8F_{17} (perfluorooctylbutane trimethylammonium bromide). Cryo-TEM shows that this surfactant self-assembles into narrow ribbons with a relatively narrow width distribution, both in salt-free solutions and in the presence of salt. The dimensions of these ribbons as determined by SAXS and cryo-TEM are approximately 40 Å × 30 Å. A SANS study shows that the local structure is independent of the nature of the salt. It is the first report to our knowledge of the formation of a population consisting only of narrow ribbons at such a low concentration ($C \approx 10^{-2}$ g/cm^3). This is likely due to antagonistic effects of the fluorinated tails that favor planar structure and the hydrogenated spacer polar heads entities that tend to confer a cylindrical shape to the micelles. Furthermore, the cryo-TEM pictures show the presence of networks of multiconnected micelles in the salt-free systems in the vicinity of C^*. This confirms previous light-scattering results.[3] The dynamical study of these systems leads to the following conclusions: First, the ribbon solutions exhibit the same shear-thickening effect, even enhanced, as the same cylindrical micelle systems. The T-jump results obtained in the dilute regime show unambiguously that the surfactant does not self-assemble into linear micelles with an exponential distribution of lengths, as predicted by the classical models. This observation may be crucial to the understanding of the puzzling shear-thickening effect. The presence of the microgels revealed by cryo-TEM, also suggested by the previous

light-scattering study, may be at the origin of the effect. The combined T-jump and rheological study also shows a strong correlation between the relaxation time associated with the main process in the T-jump experiments and the critical shear rate, thus indicating that the latter is controlled by the micellar kinetics.

LA0525832